Detailed measurements in a swirling particulate two-phase flow by a phase-Doppler anemometer

M. Sommerfeld and H.-H. Qiu
Lehrstuhl für Strömungsmechanik, Friedrich-Alexander Universität Erlangen-Nürnberg, Erlangen, Germany

The particle dispersion characteristics in a confined swirling flow with a swirl number of 0.47 have been studied in detail by applying the phase-Doppler technique, which allows the measurement of particle size and velocity. Furthermore, simultaneous measurement of the gas velocity was performed with some improvements in the data processing technique that allowed the gas velocity in presence of the dispersed phase to be obtained. From the particle velocity and size measurements the behavior of different sized classes out of the whole size spectrum ranging from about 20 to 80 μm could be studied, and the response of the particles to the mean flow and the fluid turbulence could be characterized. As a result of the complexity of the flow field and the very different time scales involved, the particle behavior was found to be a result of different phenomena. Due to the combined action of turbulent diffusion, radial particle transport, and centrifugal forces exerted on the particles, a separation of the particle phase was observed, resulting in a streamwise increasing particle mean number diameter in the core region of the flow.

Keywords: swirling flow; turbulent particle dispersion; particle size/velocity measurements

Introduction

Swirling two-phase flows are encountered in a variety of forms in many engineering applications. In industrial processing plants, for example, cyclone separators are used to clean a fluid stream from solid particles. The mechanism for the separation of the particles is the strong centrifugal force exerted on the particle in the swirling flow of the cyclone. In combustion systems the special features of swirling flows are used to establish high mixing rates between the fuel (oil spray or coal dust) and the swirling air stream and to enhance flame stability. Flame stabilization is obtained by a central recirculation zone, the resulting upstream convection of hot reaction products, and the mixing with the oncoming fuel and air stream. The occurrence of a central recirculation zone, observed at a certain critical swirl intensity, is usually referred to as vortex breakdown.

Due to the importance of swirling flows in combustion systems and their effect on combustion efficiency and pollutant emission, both reacting and nonreacting swirling flows have been the subject of research for many years.[1–8] In some of these publications[6,8] the major difference between isothermal and reacting flow has been reported, indicating that great care must be taken to simulate a reacting flow by an isothermal flow.

Compared to the large body of publications dealing with reacting and nonreacting swirling flows, only a few publications deal with particle or droplet motion and dispersion in swirling flows.[9–13] In a recent publication by Blümcke *et al.*[11] the understanding of droplet dispersion in a turbulent confined swirling flow was improved by both experimental and numerical examinations considering single droplet motion.

The velocity-size correlation of droplets in a liquid-fueled swirl burner was recently studied by Hardalupas *et al.*[13] using a phase-Doppler system. Their results demonstrate the different behavior of different sized droplets in a swirling free jet emanating from a quarl-type burner nozzle. Only the use of such modern flow-diagnostic techniques like phase-Doppler anemometry allow detailed information on particle motion in such complex flows to be obtained. This information is necessary to improve swirl-flow-based combustion systems in order to increase efficiency and reduce pollution.

A dispersed phase consisting of droplets, which may evaporate, however, does not allow the separation of aerodynamic and thermodynamic effects in a swirling flow. Therefore a stepwise increase in complexity was desired in the present study. In a preliminary study, the effect on the dispersion of solid particles in a confined swirling flow was studied in comparison to the nonswirling case.[14] In these experiments, spherical glass beads with a mean number diameter of 108 μm and a narrow size distribution were used. This implies that all the particles behave in the same way, namely, that of a monodisperse phase.

The simulation of a more realistic condition as, for example, found in coal-dust burners requires the use of a particle with a wide size distribution between 0 and about 100 μm. This article reports on measurements in a confined swirling two-phase flow by using glass beads with a mean number diameter of 45 μm distributed between 20 and 80 μm. For the characterization of the particle dispersion, an improved phase-Doppler system was established, thus allowing the simultaneous measurement of particle-size–velocity correlations and the velocity of seeding particles, which are used as indicators of the gas flow field.

Test facility

For the detailed study of swirling two-phase flows, a vertical test section with a downward flow was chosen (Figure 1). The complete test rig consists of two flow circuits (5 and 6) for the primary and secondary annular flow, respectively. A blower (1) with variable flow rate supplies these two pipe systems via a

Address reprint requests to Dr. Sommerfeld at Lehrstuhl für Strömungsmechanik, Friedrich-Alexander-Universität, Erlangen-Nürnberg, D-8520 Erlangen, Cauerstrasse 4, Germany.

Received 19 June 1990; accepted 10 September 1990

T-junction and a throttle-valve (2), whereby the flow rate of the primary inlet may be adjusted. The flow rates of the primary and annular flows are obtained from two orifice flow meters (3). The swirl intensity of the annular flow may be adjusted continuously by turning the swirl vanes in the radial swirl generator (8) to a certain degree.

The inlet configuration and the dimensions of the test section are also shown in Figure 1. The test section consists of a 1.5 m long Plexiglas tube with an inner diameter of 194 mm. The end of the test section is connected to a stagnation chamber (11), because previous measurements[8,14] showed that an area contraction at the end of the test section has a significant influence on the flow structure in the test section. This was caused by the subcritical nature of isothermal swirling flow, where the area contraction at the outlet may result in inertial waves propagating upstream against the flow, considerably influencing the flow structure.

The stagnation chamber is connected to a cyclone separator (13) and an additional filter to separate both the large particles and the seeding particles. To guarantee that the flow rate in the test section is independent of the pressure loss in the filter system, an additional blower (12) is used in connection with a bypass valve at the stagnation chamber (11). The particle flow rate in the primary jet is controlled by a feeding system consisting of a particle feeder (4) and a particle reservoir (7).

Particle size and velocity measurements are performed by a one-component phase-Doppler anemometer (PDA) at several cross sections in the test section, including the inlet. To allow for the measurement of the three velocity components (axial velocity u, radial velocity v, and tangential velocity w) the PDA-system (9) is mounted on a 3-dimensional (3-D) traversing system. To avoid strong laser beam deflections and a realignment of the receiving optics for every measuring point the Plexiglas test section has several slits that are closed by thin, 100 μm glass plates. This results in negligible beam distortion, especially when the radial and axial size–velocity correlation is measured, where the receiving optics has to be mounted in such a way that the optical axis is oblique to the walls of the test section.

Measuring technique

The phase-Doppler system used for the present experiments is shown in Figure 2 together with the data processing system. The transmitting optics is a conventional system with two bragg cells and a front lens with 485 mm focal length. The phase-Doppler receiving optics is mounted at 30° off axis from the forward scattering direction. For the measurement of the axial velocity and the radial and tangential velocity, the receiving optics has different positions, and test sections with different slit locations are used.

By using a system of three lenses the scattered light from the particles is focused onto the pinholes in front of two avalanche photodiodes (Figure 2) with a separation of 40 mm. This results in a measurable particle size up to 123.8 μm. A summary of the optical parameters and the dimensions of the measuring volume are given in Table 1.

The signals from the two avalanche photodiodes are band-pass filtered and stored in a 200-MHz two-channel transient recorder (type: Le Croy 8013 A). The transient recorder is operated in a sequential mode, where the total storage of 32 Kbyte for each channel was divided into 400 segments by an external trigger unit. After storage of the 400 burst pairs, the data are transferred to a Compaq 386/25 personal computer by an IEEE-488 interface card. While the data are processed

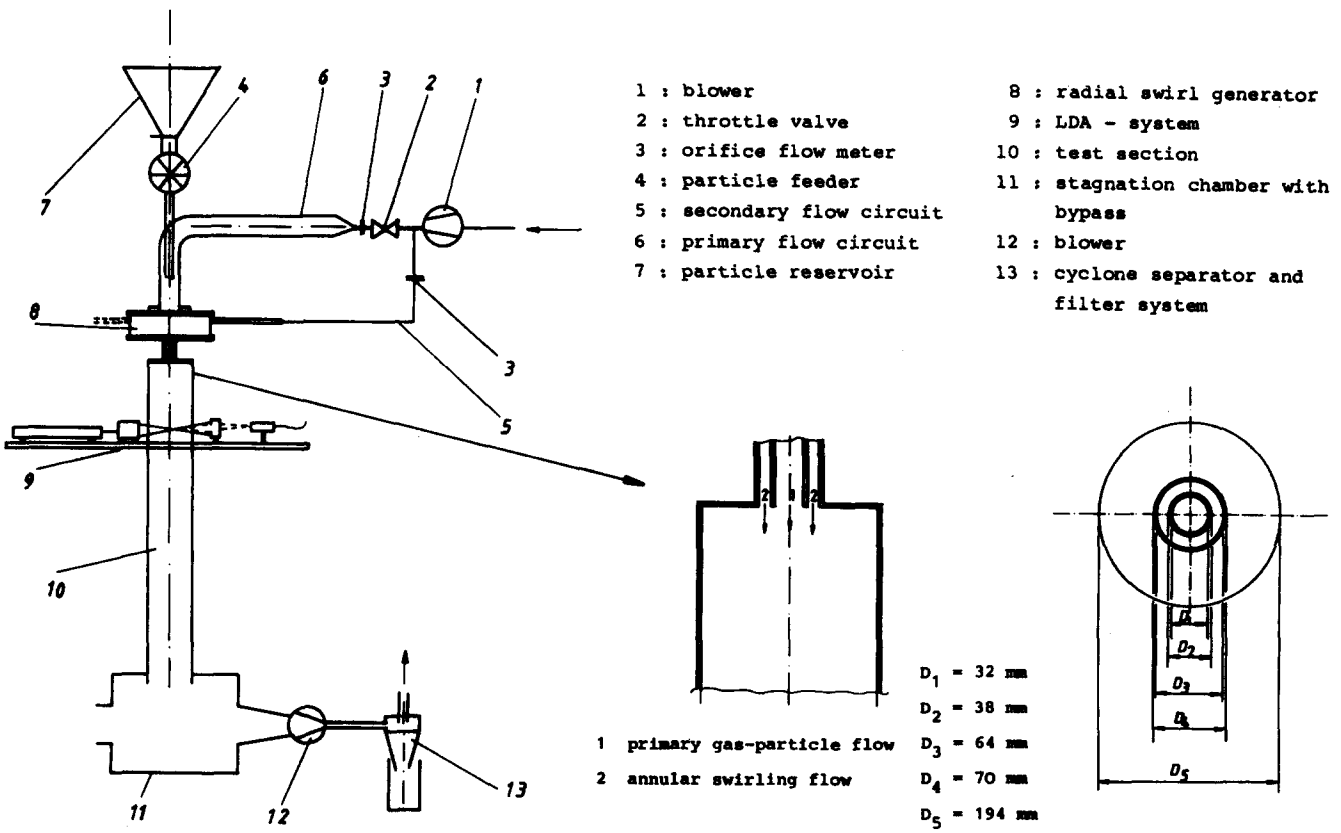

Figure 1 Schematic drawing of test facility and test section with dimensions

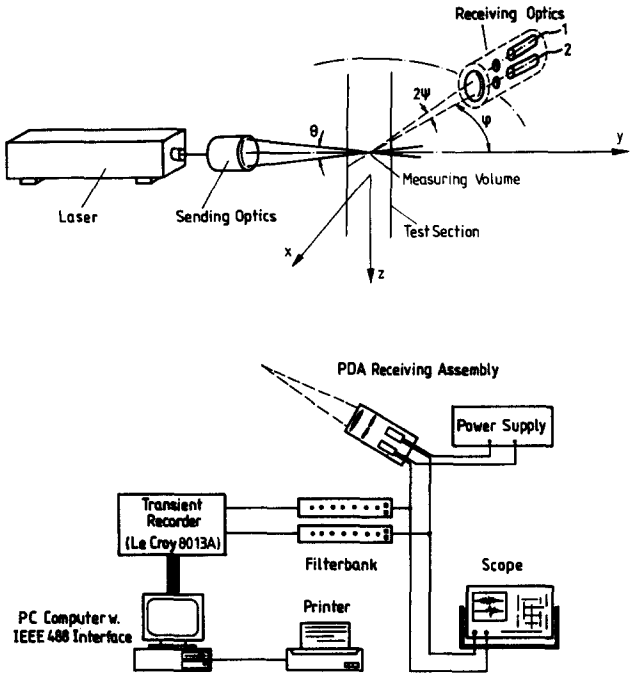

Figure 2 Phase-Doppler system with data acquisition

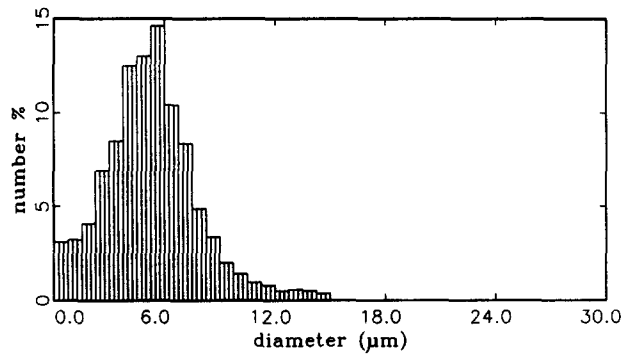

Figure 3 Size distribution of seeding particles

in the PC, the next 400 burst pairs are stored in the transient recorder. By this procedure it is possible to achieve effective data rates of about 50 Hz. The data processing used to evaluate phase and frequency is based on the cross-spectral density function in connection with a fast-Fourier transform (FFT),[15] which was recently modified to give higher accuracy for the velocity estimation by using improved Gaussian interpolation functions.[16]

The FFT length was set to 64 points, with a sampling frequency of 12.5 MHz. This rather short FFT length gave high processing speeds, and accuracies between 0.07 and 0.15 m/s could be achieved for velocity estimation. The accuracy for size measurements was in the range of 0.8 to 0.25 μm. These values cover the range of the signal-to-noise ratios measured in the present situation. More details about the accuracy, which strongly depends on the signal-to-noise ratio, are given in Reference 16.

The phase-Doppler anemometry (PDA) allows the simultaneous measurement of size and velocity of spherical particles, droplets, or bubbles. Until now this measuring technique has been mainly applied to characterize spray systems,[17,18] where only the size and velocity of the droplets are of interest. In complex two-phase flows and at higher particle loadings, however, we are interested in measuring the velocity of the continuous phase in presence of the dispersed phase in addition to the size of the particles. Although such applications of the phase-Doppler technique are still rare, some suggestions are given in the literature.[19,20]

The principal idea in the present study is to use the phase information to distinguish between signals from seeding particles and dispersed-phase particles. A necessary condition for allowing seed measurements by the phase-Doppler method is that the seeding particles are spherical and have the same optical quality as the big particles, namely, the refractive index must be identical. Therefore in the present experiments small spherical glass beads (Ballotini type 7000) are used. The size distribution of the seeding particles is shown in Figure 3. Other conventional seeding materials, such as MgO or Al_2O_3 are not adequate for phase-Doppler measurements, since even for small nonspherical particles there will be a cross-talk with the big particles, resulting in size and velocity measurement errors.

The size distribution of the seeding glass beads ranges from about 0 to 10 μm, but only particles up to about 4 μm are sampled for the seeding measurements by the phase discrimination procedure.

The main problem encountered for this discrimination is the occurrence of oscillations in the phase–size relation in the range of particle sizes below 10 μm. A solution to this problem was suggested by Hardalupas and Taylor,[19] where a phase limitation was applied in order to avoid counting larger particles as seeding particles. This method has also been used in the present experiments. The phase–size relation obtained from a Mie calculation[21] for the present optical configuration including integration over the circular apertures, is shown in Figure 4. Here ϕ_{max} is the maximum of the phase for validating seeding particles with a diameter of less than about 4 μm. Since the probability of sampling particles of less than 2.5 μm is much higher (Figure 4), the mean diameter of the validated seeding particles is about 1.5 μm.

For simultaneous measurement of seeding and dispersed-phase particles, one additional problem arises, stemming from the use of a definite trigger level and gain. Since the amplitude of the seeding signals is much lower than that of the big particles, a simultaneous measurement would require a low trigger level. This implies that the signals of the big particles are triggered at the very beginning of the burst, which results in a poor signal-to-noise ratio and some phase errors resulting from trajectory dependent effects.[22]

Therefore the measurements are performed in the following

Table 1 Parameters of the optical system

Transmitting optics	
Wave length of the laser	632.8 nm
Diameter of laser beam	1.0 mm
Focal length of front lens	485 mm
Beam separation	30 mm
Diameter of measuring volume	391 μm
Length of measuring volume	12.6 mm
Fringe number	38
Conversion factor	10.24 m/s/MHz
Receiving optics	
Off-axis angle	30°
Focal length of receiving lens	310 mm
Detector separation	40 mm
Diameter of pinhole mounted in front of the photodiodes	200 μm
Length of measuring volume imaged onto the photodiodes	775 μm
Phase conversion factor	$-2.93°\ \mu m^{-1}$

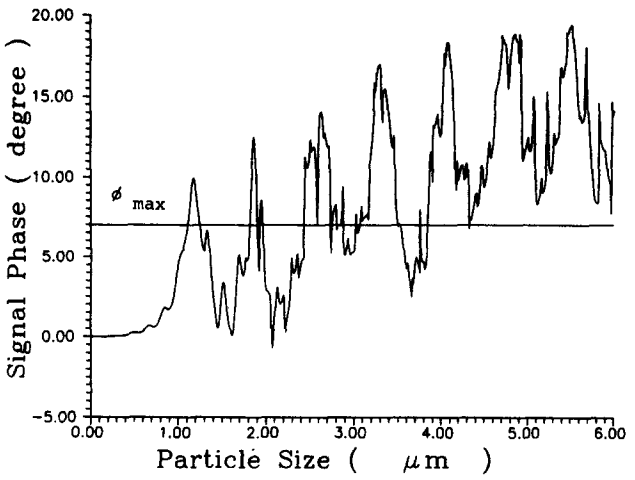

Figure 4 Mie calculation of phase-size relation

procedure. In the first stage only the required number of seeding signals are sampled using a low trigger level and a high gain at the transient recorder. The signals from the big particles with a phase larger than 7° are rejected during this measuring period. Thereafter the trigger level and the gain of the transient recorder are automatically increased and reduced, respectively, and the required number of samples for the big particles are acquired. The signals from the seeding particles (phase smaller than 7°) are either below the trigger level or rejected by the software during this period. This procedure allowed the measurement of the gas phase in presence of the dispersed phase and the use of variable gain ensured a good amplitude resolution of the signals.

The particle mass flux was measured separately with a single detector receiving system. This receiving optics was positioned 90° off axis from the forward scattering direction in order to obtain an exact demarcation of the measuring volume. At each measuring point the number of particles N traversing the control volume were counted within a certain time period, Δt. Simultaneously, the particle velocity was measured. For these measurements the transient recorder was also operated in the sequential mode, which ensured a fast enough data acquisition. During the storage of the 400 events, an internal clock was used to determine the effective measuring time, Δt. The total particle mass flux is then obtained with the cross section of the control volume A_c, which was calculated from the optical configuration:

$$f=\frac{N\bar{m}_p}{\Delta t A_c}$$

The mean particle mass at a certain measuring location is obtained from the phase-Doppler measurements. Due to the uncertainties in the determination of the cross section of the control volume, the measured mass flux was corrected using the global mass balance. Therefore the total particle mass flow rate at the inlet was obtained by integrating the mass flux profile. In comparison with the global mass flow rate obtained by weighing the particles collected during a certain time period, a correction factor was determined and applied to the mass flux measurements in all other cross sections.

Furthermore, the particle mass flux was separated to give the positive and negative fluxes, which provides additional information about the amount of particles having negative velocities. For this separation the particle mean diameter for particles with only positive and negative axial velocity was determined from the PDA measurements.

Flow conditions

For the present experiments the flow rates in the primary and and the annular inlet are adjusted to give maximum velocities of 12.5 m/s and 18 m/s, respectively. The associated mass flow rates, the flow Reynolds number, the swirl number, and other experimental conditions are listed in Table 2. The mass flow rates of the primary and annular, secondary jets are calculated from the pressure drops across the orifice flow meters. The flow Reynolds number was obtained with the total volume flow rate at the inlet and the outer diameter of the annulus. The swirl number was calculated as the ratio of the axial flux of angular momentum to the axial flux of linear momentum, which is obtained by integration across both the primary and annular inlet. The following definition of the swirl number is used:

$$S=\frac{2\int_0^{D_3/2}\rho w u r^2\,dr}{D_5\int_0^{D_3/2}\rho u^2 r\,dr}$$

The properties of the glass beads and the particle flow rate also are given in Table 2. The particles have a smooth surface and are spherical in shape. Less than 2% of the particles are nonspherical or fragments (Figure 5a), which results in only small errors in sizing the beads. Therefore this particle material is ideal for phase-Doppler measurements. The particle-size distribution obtained by a phase-Doppler measurement (20,000 samples) is given in Figure 5b.

Since during the experiment some of the smaller particles were not collected in the cyclone separator but got caught in the paper filter, the particle material was frequently renewed in order to guarantee that the particles always have the same size distribution. This was ensured by controlling the particle size distribution at the inlet from time to time. Effects of particle damage as reported by Hardalupas *et al.*[23] could not be observed in the present measurements.

Experimental results and discussion

Measurements of the three velocity components were conducted at seven cross sections downstream of the inlet. At each measuring location 2,000 samples were taken to obtain the gas velocity and the associated rms values. In order to achieve reasonably accurate velocity statistics for the particle phase in the different size classes, 20,000 samples were acquired. The total measuring time for each location was between 15 and 30 min, which was strongly dependent on the local particle concentration. The particle size distribution in the range between 0 and 123.8 μm was resolved by 40 classes of 3.1 μm width.

Table 2 Flow conditions

Air flow	
Mass flow rate of primary jet	9.9 g/s
Mass flow rate of secondary jet	38.3 g/s
Inlet Reynolds number (obtained with $D=64$ mm)	52400
Swirl number	0.47
Particles	
Particle mean number diameter	45.5 μm
Particle material density	2500 kg/m³
Particle mass flow rate	0.34 g/s
Particle loading	0.034

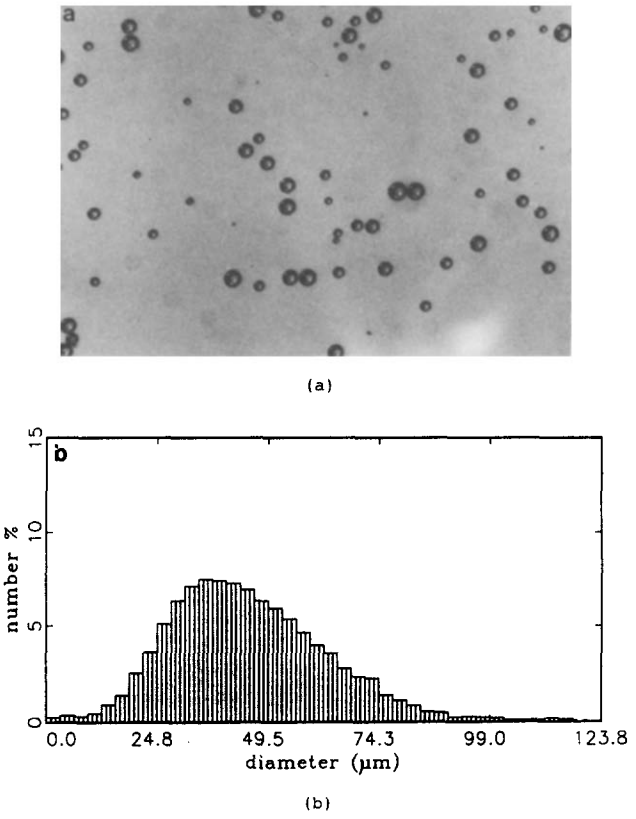

Figure 5 (a) Photograph of glass beads; (b) particle size distribution

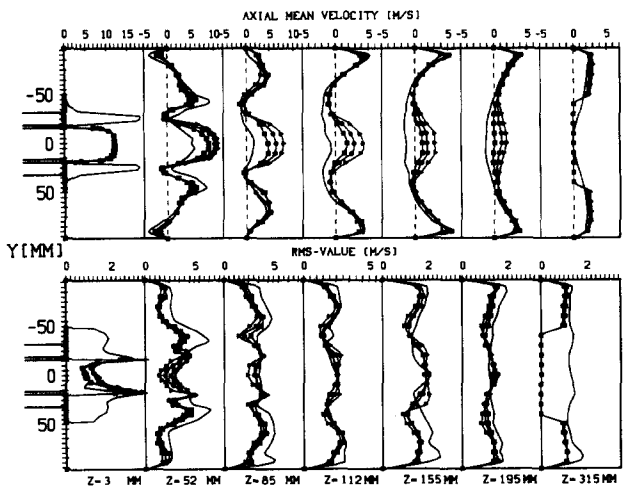

Figure 6 Axial mean velocity and rms values of air and particles, (——— air; particles: □ 30 μm, ○ 45 μm, and △ 60 μm)

Besides the information on the change of the particle-size distribution throughout the flow field, the stored data of particle size and velocity could be reprocessed after the measurement to give the particle velocity in a certain size range. In Figure 6 (and later in Figures 10 and 11) the axial, tangential, and radial velocities together with the associated rms values are shown for the air flow and three particle size classes (30, 45, and 60 μm) of 10 μm width.

Considering the axial air velocity (Figure 6), it is seen that the central recirculation region ranges from about 80 to 330 mm downstream of the inlet. Due to the rapid expansion of the annular air jet, which is a special feature of swirling flows,[2,24] the recirculation region in the edges of the pipe expansion only extends to about 100 mm.

A clearer picture of the gas flow field may be obtained by calculating the gas-phase stream functions by integrating the axial velocity profiles and applying an interpolation procedure. The plot of the gas-phase stream function is shown in Figure 7. The highest negative velocities within the recirculation bubble are found at the location $z=120$ mm and $y=\pm 35$ mm (see Figure 6). This location ($z=120$ mm) is associated with the maximum width of the central reverse flow region. Farther downstream the diameter of the recirculation region is continuously reduced.

The particles that initially have about the same velocity as the air flow are not able to follow the rapid expansion and deceleration of the air jets. Therefore the particles have much higher velocities than the air flow in the core of the test section and almost penetrate the central reverse flow region. Due to their higher inertia, the larger particles have the higher velocities. Only the smaller particles in the size spectrum ($D_p=30$ μm) attain slightly negative mean velocities in the core region at about 195 mm downstream of the inlet. At the edges of the central recirculation of the air flow, however, an annular-shaped particle recirculation region develops at about 50 mm downstream of the inlet and increases in width further downstream. This annular area of negative, axial mean particle velocity is within the mixing region between the primary and annular jet, where the particle motion is strongly controlled by turbulent diffusion. In the region of the coflowing, swirling air stream, which initially has a higher velocity as the primary jet, the particles have about the same velocity as the air flow up to about $z=200$ mm.

The axial turbulent velocity fluctuation of the particles is initially lower than the fluid fluctuation, and the smaller particles in the size spectrum exhibit the higher fluctuations that are closer to the values of the air flow ($z=52$ and 85 mm). From about 85 mm downstream of the inlet, the particles' velocity fluctuation becomes higher than the fluid turbulent fluctuation in the core region of the test section, which is in the center part of the central recirculation bubble.

This is caused by the fact that particles with completely different histories throughout the flow field pass a measuring location within the central part of the recirculation region. Obviously a number of particles that issue from the primary inlet traverse rather straight through the recirculation bubble and, additionally, particles recirculate with the air flow. Additionally, particles recirculating in the region of flow reversal at the edge of the pipe expansion may pass through the central recirculation bubble due to inertial effects. This rather complicated particle behavior could be explained in detail only by

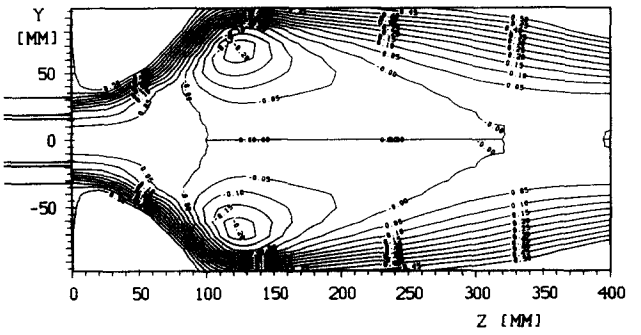

Figure 7 Gas-phase stream function

using a two-component PDA system, which allows determination of the correlation between axial and radial velocity and hence the orientation of the particle trajectories. Unfortunately, such a system was not available for the present studies.

However, a more detailed consideration of the experimental results may assist in understanding and explaining the presence of the historical effects mentioned. Therefore in Figure 8 the measurements of the particle size distribution with the associated axial mean velocities and velocity fluctuations in the respective size classes are shown for two representative locations in the flow field. Furthermore, the joint velocity distribution of all classes of the dispersed-phase particles is given. Separation of this velocity PDF allows us to distinguish between those particles having positive and negative velocities. The corresponding size distributions of particles with only positive and negative velocities are also given in Figure 8.

The measurement obtained at $z=112$ mm, $y=20$ mm indicates that there must be at least two preferential particle trajectories and histories. The recirculating particles have almost constant velocities in all classes and are smaller than the particles with positive velocities. The size distribution of the particles with positive velocities is wider and the mean diameter is higher than for particles with negative velocities. Due to inertial effects, a correlation between particle size and velocity still is present, indicated by the increasing velocity with size.

Similar phenomena are observed at ($z=195$ mm, $y=0$ mm). At this location the particles with positive velocities are even larger as a result of the separation effect, which will be described later. Also at this location, the probability of larger particles having negative velocities exists. Finally, it should be mentioned that the scale of the particle number in Figure 8 is only a relative measure: It is different for particles with negative and positive velocities.

Also the higher velocity fluctuations of the larger particles compared to the smaller ones at $z=112$ and $z=155$ mm is a result of the historical effect, since the majority of larger

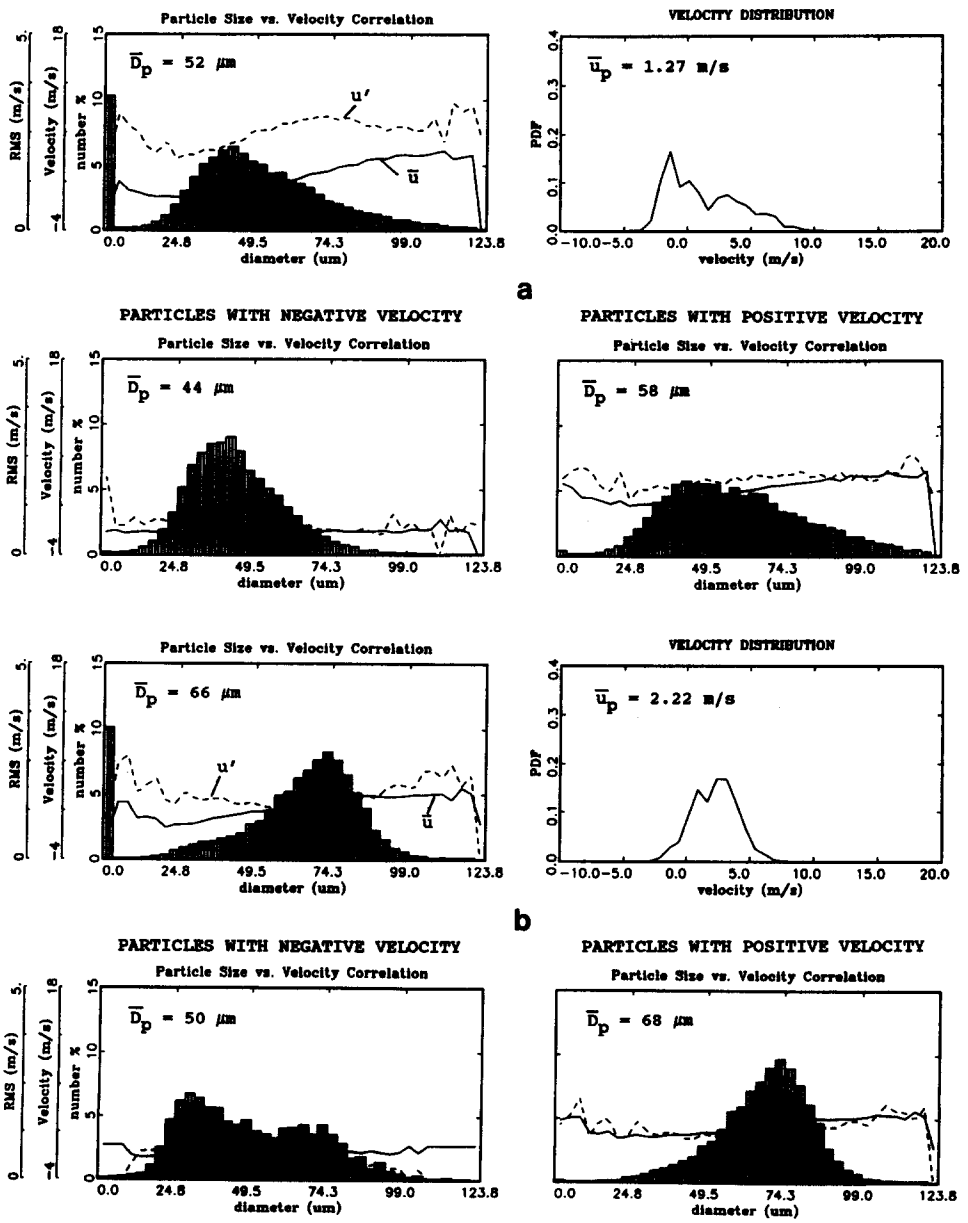

Figure 8 Particle size distributions for particles with positive and negative velocities: (a) $z=112$ mm, $y=20$ mm; (b) $z=195$ mm, $y=0$ mm

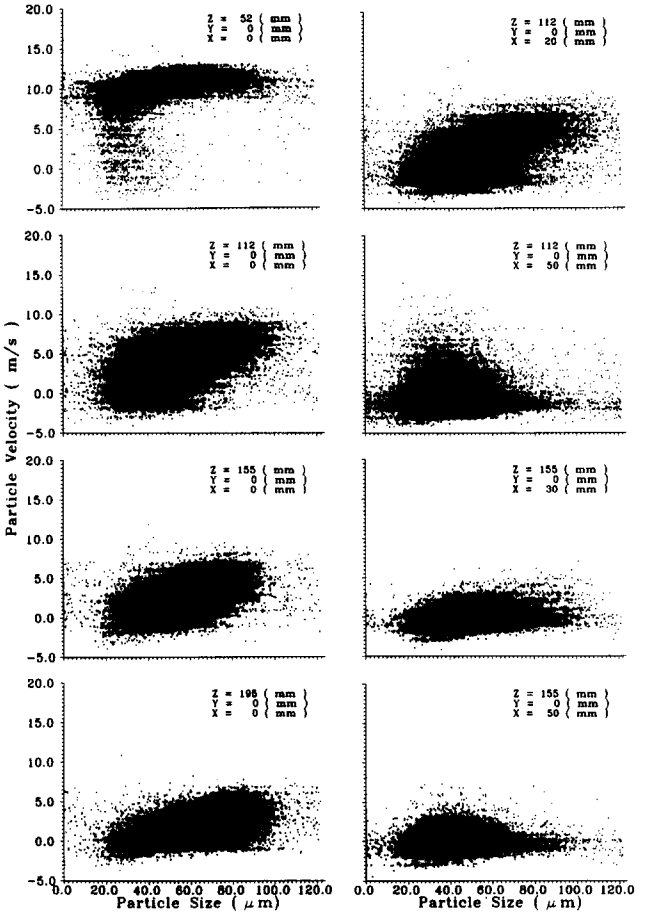

Figure 9 Measured particle-size–velocity correlations at different locations in the flow field

particles have the tendency to pass straight through the recirculation zone with a rather high velocity due to their inertia. Additionally, however, larger particles, which respond to the flow reversal only farther downstream, are moving upstream with the flow (see Figure 8). This results in much wider velocity distributions for the larger particles compared to the smaller ones, which fairly soon—after issuing from the inlet—are decelerated by the air flow and hence have lower positive axial velocities.

These effects may be identified by considering the measured correlation between particle size and velocity (Figure 9), where each plotted point represents one sample of the 20,000 total samples. It is evident from these plots that the velocity distribution for the larger particles is wider than for the smaller ones at the locations ($z=112$ mm, $y=20$ mm), ($z=155$ mm, $y=30$ mm), and ($z=195$ mm, $y=0$). Especially at the location ($z=112$ mm, $y=20$ mm) the number of particles with negative velocities is about the same for particles in the range between 20 and 60 μm. The motion of even larger particles is dominated by inertial effects, and they have mainly positive axial velocities of about 5 m/s.

Therefore these results are a clear indication of the phenomenon described. The measured velocity fluctuation of the particles is not a result of the inlet conditions and the interaction with the fluid turbulence alone but also exhibits the uncorrelated particle motion, since particles with different histories through the flow field are sampled at one measuring location.[25,26]

Additionally, Figure 9 shows the development of the correlation between particle size and velocity along the centerline. These results indicate clearly that the smaller particles rather soon respond to the recirculation of gas flow. Furthermore, the velocity distributions of the smaller particles are much wider at $z=58$ mm and $z=112$ mm than for the larger particles, which indicates their response to the fluid turbulence. This results in higher rms values of the axial velocity for the smaller particles at these locations (see Figure 6).

Outside the core region of the recirculation bubble, the turbulence intensity of the fluid is higher than the velocity fluctuation of the particles, where the smaller ones have the higher fluctuations (see Figures 6 and 9).

The measurements of the tangential velocity (Figure 10) reveal the typical vortex structure observed in swirling flows. The maximum of the tangential air velocity at the secondary inlet is about 14 m/s, rapidly decays to about 2 m/s at $z=112$ mm, and again increases to about 3 m/s at the end of the central recirculation zone. From the beginning of the central recirculation region the gas velocity profiles show an almost linear increase of the tangential velocity in the core region of the test section, which is similar to solid-body rotation. Outside this area free vortex behavior may be identified.

The particles are not able to follow the rotation of the air flow and therefore have lower tangential velocities throughout the test section. The slip between particles and air flow increases with particle diameter. Except for the inlet and at $z=52$ mm, the rms values of the tangential air velocity are rather constant in the radial direction and decay slightly in the downstream direction.

Only the radial velocity could be measured for half a cross section (Figure 11). However, since the symmetry of the flow is reasonably good (see Figures 6 and 10), it may be expected that the radial velocity profiles are symmetric.

The strong spreading of the air jet caused by the swirl results in high radial velocities at $z=52$ mm and $z=85$ mm. At about 112 mm downstream of the inlet, the location of the maximum width of the central recirculation region is reached (see Figure 7), and the radial velocity becomes smaller. Due to the particles' inertia, they maintain—after an initial acceleration—a higher outward directed radial velocity. Farther downstream, where the width of the recirculation region is reduced, the air flow is directed inward toward the axis. Only some small particles are able to follow this inward motion (at $z=155$ mm and $z=195$ mm). Owing to the centrifugal forces exerted on the particles in a swirling flow, however, most particles are transported outward and finally accumulate near the wall (Figure 12).

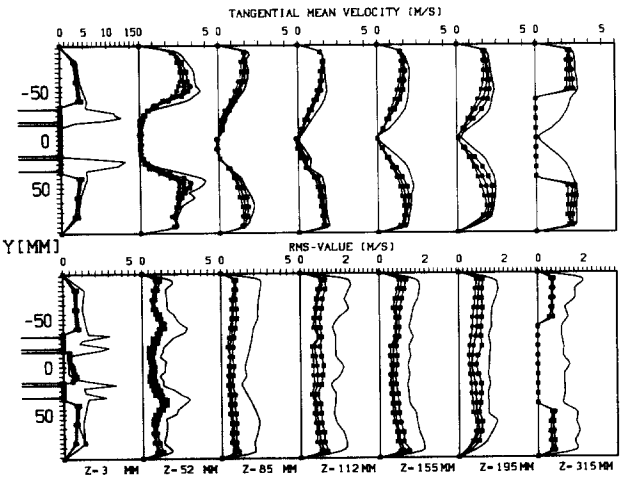

Figure 10 Tangential mean velocity and rms values of air and particles, (——— air; particles: □ 30 μm, ○ 45 μm, and △ 60 μm)

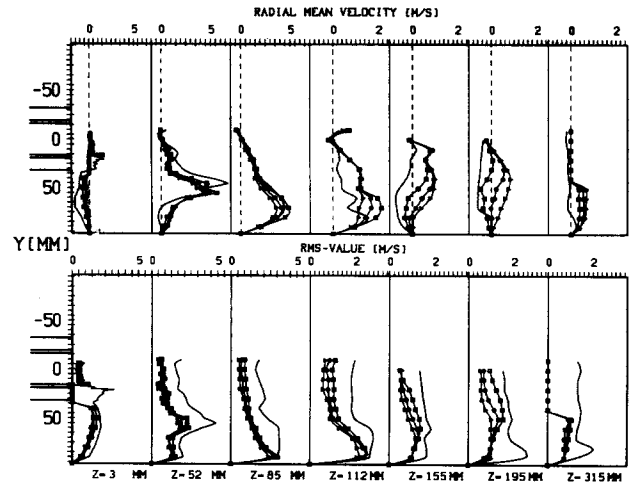

Figure 11 Radial mean velocity and rms values of air and particles, (——— air; particles: □ 30 μm, ○ 45 μm, and △ 60 μm)

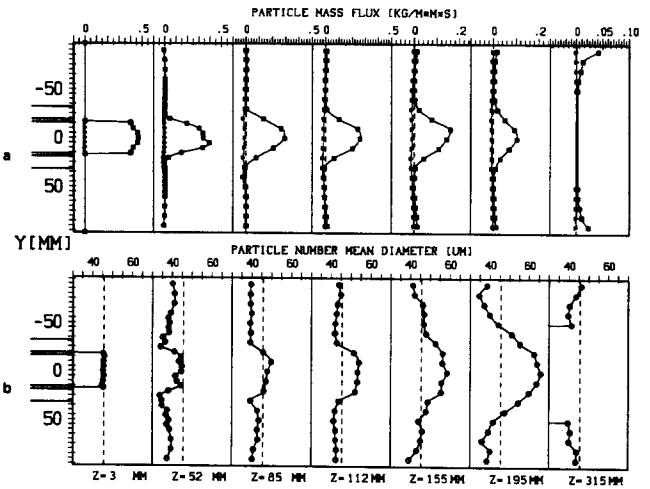

Figure 12 (a) Particle mass flux (□ total and △ negative flux); (b) development of the particle mean number diameter

In addition to the particle velocities in different size classes, the particle behavior in the swirling flow may be characterized by considering the particle mass flux distribution and the development of the particle mean number diameter throughout the flow field (Figure 12). In order to show the number of recirculating particles that have negative velocities, the particle mass flux is separated into a negative and a total flux (Figure 12a).

Only a small mass fraction of particles are recirculating within the central reverse-flow region, and the maximum of the negative flux appears at the edge of the particle jet. The majority of the particles penetrate the central reverse-flow region, and the maximum in the particle mass flux remains near the center (up to $z=200$ mm). From about $z=112$ mm the particle mass flux near the wall begins to increase, due to the effect of radial transport, turbulent diffusion, and centrifugal forces. At $z=315$ mm all the particles are removed from the core region and accumulate near the wall.

The distribution of the particle mean number diameter (Figure 12b) demonstrates the separation effects in a swirling flow. In a region where the particles issuing from the primary jet have not yet achieved a considerable tangential velocity, the smaller particles are transported outward in the radial direction due to the high radial air velocities and the associated drag force. Additionally, turbulent diffusion plays an important role for particles near the edge of the particle jet, since they pass through the shear layer between primary and annular jet. In this initial stage, centrifugal forces are not yet important since the particles did not acquire a considerable tangential velocity (see Figure 10). The larger particles maintain their initial straight motion due to their large inertia and penetrate a large part of the recirculation bubble. Only a few large particles are able to respond to the flow reversal and have negative velocities. However, due to increasing centrifugal force and radial transport, the large particles are finally removed from the core region. These effects result in an increasing particle mean diameter in the core region of the swirling flow (Figure 12b) and the presence of only smaller particles in the outer region. Even though a swirling flow is already very complex itself, it is believed that the present results may give a clear picture of the complex particle behavior and motion in such a flow situation.

Conclusion

Detailed studies of the aerodynamics of a particle-laden, confined swirling flow using the phase-Doppler anemometry revealed the behavior of different sized particles in a complex flow. In addition, the spatial change of the particle-size distribution throughout the flow field was obtained. Due to the aerodynamic transport of the particles, turbulent diffusion, and centrifugal effects, a separation of the particle phase was observed. This resulted in a streamwise increasing particle mean diameter in the core region of the flow.

From the particle flux measurements and the separation of the particle velocity distribution into particles with positive and negative velocities, it was found that only a small amount of particles recirculate within the closed central reverse-flow region of the gas.

The measured axial particle velocity fluctuations in the core part of the recirculation bubble were found to be higher than the fluid turbulence. This phenomenon is associated with the uncorrelated particle motion, being the result of inertial and historical effects. This observation is typical for complex flows with flow reversal, where particles with completely different histories in the flow pass through the same measuring location.

The experimental results are now going to be used for improving numerical prediction methods for turbulent, swirling two-phase flows. In a continuation of the present work, the dispersion of evaporating droplets will be studied, where the particle transport is influenced by heat and mass transfer in addition to aerodynamic effects.

Acknowledgment

The financial support of the project "Heterogeneous combustion in swirling flows: Particle dispersion with heat and mass transfer" by the Stiftung Volkswagenwerk is gratefully acknowledged. The authors also would like to thank D. Koubaridis, who performed a major part of the experiments for his diploma thesis.

References

1 Syred, N. and Beer, J. M. Combustion in swirling flow: A review. *Comb. and Flame*, 1974, **23**, 143–201

2 Kuroda, C. and Ogawa, K. Characteristic flow behaviour of high swirling jet in a circular vessel. *J. Chem. Eng. Japan*, 1987, **20**, 188–190

3 Brum, R. D. and Samuelson, G. S. Two-component laser anemometry measurements of non-reacting and reacting com-

plex flows in a swirl-stabilized model combustor. *Exp. in Fluids*, 1987, **5**, 95–102
4 Hallett, W. L. H. and Toews, P. J. The effect of inlet conditions and expansion ratio on the onset of flow reversal in swirling flow in a sudden expansion. *Exp. in Fluids*, 1987, **5**, 129–133
5 Altgeld, H., Jones, W. P., and Wilhelmi, J. Velocity measurements in a confined swirl driven recirculating flow. *Exp. in Fluids*, 1983, **1**, 73–78
6 Lilley, D. G. Swirl flow in combustion: A review. *AIAA J.*, 1977, **15**, 1063–1078
7 Vu, B. T. and Gouldin, F. C. Flow measurements in a model swirl combustor. *AIAA J.*, 1982, **20**, 642–651
8 Escudier, M. P. and Keller, J. J. Recirculation in swirl flow: A manifestation of vortex breakdown. *AIAA J.*, 1982, **20**, 642–651
9 Thielen, W. Einfluss der Brennerkonstruktion auf das brennernahe Stömungsfeld in gestuften Kohlestaubfeuerungen. Brennst. *Wärme Kraft*, 1988, **40**, 186–192
10 Farac, T. M., Arai, M., and Hiroyasu, H. Effects of fuel volatility on spray combustion. *Proc. 19th Symp. (Int.) on Combustion*, The Combustion Inst., 1982, 511–518
11 Blümcke, E., Eickhoff, H., and Hassa, C. Dispersion of monosized droplets in a turbulent swirling flow. *Proc. 4th Int. Conf. on Liquid Atomiyation and Spray Systems*, 1988, 89–96
12 Truelove, J. J. The modelling of flow and combustion in swirled pulverized-coal burners. *Proc. 20th Symp. (Int.) on Combustion*, The Combustion Institute, 1984, 523–530
13 Hardalupas, Y., Taylor, A. M. K. P., and Whitelaw, J. H. Velocity and size characteristics of liquid-fuelled flames stabilized by a swirl burner. *Proc. Royal Soc. London*, 1990, **A428**, 129–155
14 Sommerfeld, M. and Krebs, W. Particle dispersion in a swirling confined jet flow. *Part. and Part. Syst. Charact.*, 1990, **7**, 16–24
15 Domnick, J., Ertel, H., and Tropea, C. Processing of Phase/Doppler Signals using the cross spectral density function. *Proc. 4th Int. Symp. on Appl. of Laser Anemometry to Fluid Mech.*, Paper 3.8, 1988
16 Qui, H.-H., Sommerfeld, M., and Durst, F. High resolution data processing for Phase-Doppler measurements in a complex two-phase flow. *Proc. 5th Int. Symp. on Appl. of Laser Tech. to Fluid Mech.*, Paper 24.2, 1990
17 Bachalo, W. D. and Houser, M. J. Evolutionary behavior of sprays produced by pressure atomizers. AIAA Paper 86-0296, 1986
18 Bhatia, J. C., Domnick, J., Durst, F., and Tropea, C. Phase-Doppler-anemometry and the log-hyperbolic distribution applied to liquid sprays. *Part. and Part. Syst. Charact.*, 1988, **5**, 153–164
19 Hardalupas, Y. and Taylor, A. M. K. P. The identification of LDA seeding particles by the phase-Doppler technique. *Exp. in Fluids*, 1988, **6**, 137–140
20 Bachalo, W. D., Sankar, S. V., Weber, B. J., and Rudoff, R. C. Advances in the diagnostics for research in turbulent steady and unsteady two-phase flows. *Proc. Int. Conf. on Mech. of Two-Phase Flows*, Taipei, Taiwan, 1989, 73–78
21 Naqwi, A. and Durst, F. Computation of light scattering from a dual-beam system. LSTM Erlangen, Report LSTM/259/T/89, 1989
22 Saffman, M. Optical particle size using the phase of LDA signals. DANTEC Information, No. 5, 1987
23 Hardalupas, Y., Taylor, A. M. K. P., and Whitelaw, J. H. Measurements in heavily-laden dusty jets with phase-Doppler anemometry. *Proc. 2nd Int. Symp. on Transport Phenom. in Turb. Flows* (Hirata, M. snd Kasagi, M., Eds.), 1987, 821–835
24 Rhode, D. L., Lilley, D. G., and McLaughlin, D. K. Mean flow field in axisymmetric combustor geometries with swirl. *AIAA J.*, 1983, **21**, 593–600
25 Sommerfeld, M. Particle dispersion in turbulent flow: The effect of particle size distribution. *Proc. Int. Conf. on Mech. of Two-Phase Flows*, Taipei, Taiwan, 1989, 51–56
26 Rogers, C. B. and Eaton, J. K. The interaction between dispersed particles and fluid turbulence in a flat-plate turbulent boundary layer in air. Stanford University, Report No. MD-52, 1989